Unidirectional hopping transport of interacting particles on a finite chain

Mario Einax,[1,2,a)] Gemma C. Solomon,[3] Wolfgang Dieterich,[4] and Abraham Nitzan[2]
[1]*Institut für Physik, Technische Universität Ilmenau, 98684 Ilmenau, Germany*
[2]*School of Chemistry, Tel Aviv University, Tel Aviv 69978, Israel*
[3]*Department of Chemistry, Northwestern University, Evanston, Illinois 60208, USA*
[4]*Fachbereich Physik, Universität Konstanz, 78457 Konstanz, Germany*

(Received 5 May 2010; accepted 21 June 2010; published online 2 August 2010)

Particle transport through an open, discrete one-dimensional channel against a mechanical or chemical bias is analyzed within a master equation approach. The channel, externally driven by time-dependent site energies, allows multiple occupation due to the coupling to reservoirs. Performance criteria and optimization of active transport in a two-site channel are discussed as a function of reservoir chemical potentials, the load potential, interparticle interaction strength, driving mode, and driving period. Our results, derived from exact rate equations, are used in addition to test a previously developed time-dependent density functional theory, suggesting a wider applicability of that method in investigations of many particle systems far from equilibrium.
 [doi:10.1063/1.3463000]

I. INTRODUCTION

Random motion of a classical particle in a potential that breaks spatial inversion symmetry and fluctuates in time generally leads to unidirectional flow. On the molecular level, many important processes in biology and nanotechnology rely on this mechanism. Biological motors produce mechanical work from metabolic energy in order to affect intracellular transport, or self-propulsion of bacteria through rotatory flagellar motion.[1] Another process ubiquitous in any living organism is active transport of molecules or ions against a chemical potential gradient. Such molecular or ionic pumps generally consist of a specific channel across a cell membrane. The internal binding sites of the channel are linked to conformational fluctuations, stimulated by metabolic energy or by light.[2–5] Similar processes are known for artificial nanopores, with potential applications in molecule or ion separating devices.[6,7] In the realm of quantum transport, a net electron drift under an applied ac driving signal can be generated by various mechanisms, which may become analogous to classical unidirectional transport when dissipation is included.[8,9]

Our goals in this paper are twofold. First, we set up a model that describes unidirectional transport along a finite open system, represented by a nonsymmetric discrete chain with time-dependent driving. This model emphasizes (i) coupling of the two chain ends to reservoirs and (ii) interaction effects between transported particles that occupy the chain. These combined features distinguish our study from most works on Brownian ratchets, reviewed in Refs. 10 and 11. Indeed, both interacting Brownian motors[12–16] and ion pumping mechanisms that involve multiple occupation of the associated channel structure[4] have become important subjects of research in nonequilibrium statistical physics and biophysics. The model we examine allows us to study production of both mechanical and chemical work. In what follows we refer to a machine working against a mechanical force as "motor" and to that working against a chemical load as a "chemical pump."[1] Accordingly, attention will be focused on the system performance in both modes of operation and its dependence on the driving characteristics and on fundamental input parameters such as chemical potentials of the reservoirs, load potential, and interaction strengths. Although our model is certainly far from describing realistic systems, we argue below that at a qualitative level, the effects of concentration and interaction evaluated here should have rather general validity.

Our second goal is to provide a test of time-dependent density functional theory[17–19] (TDFT) when applied to far from equilibrium dynamics under time-dependent driving signals.[20] This method can be regarded as a version of dynamic mean-field theory, constructed such that it can account for exact static properties. Its accuracy in predicting transport properties as envisaged here will be assessed by a comparison with numerical solutions of the underlying master equation for short chains containing four sites. The numerical effort needed for such solutions increases exponentially with system size (expressed here by the number of sites between the left and right reservoirs). For this reason, establishing the validity of an approximate solution is important for future applications.

After defining our model in Sec. II, we present in Sec. III a minimal description in terms of a four-site model. Section IV introduces the TDFT method, while Sec. V examines its accuracy in comparison to "exact" numerical solutions. Also in Sec. V we present results concerning the performance of the system studied, focusing on the efficiency of its operation either as a motor working against a mechanical or electrical load, or as a chemical pump acting against a chemical bias. Section VI concludes.

[a)]Electronic mail: mario.einax@tu-ilmenau.de. URL: http://www.tu-ilmenau.de/theophys2.

II. MODEL

Our system is a one-dimensional (1D) "Fermionic" lattice gas with sites $l=1,\ldots,M$, time-dependent site energies $\varepsilon_l(t)$, nearest neighbor hopping, and a nearest neighbor interaction V. By considering a Fermionic lattice gas, equivalent to local hard core repulsions, effects of saturation of site occupations are automatically included. The sites $l=1$ and M can exchange particles with left and right reservoirs, L and R, that are sometimes represented below by indices 0 and $M+1$, respectively. We assume that these reservoirs exchange particles with the system with characteristic specified rates, but we disregard interactions between particles in the systems and those in the reservoirs, i.e., $V_{0,1}=V_{M,M+1}=0$. By definition, reservoir particles are always in equilibrium and have fixed mean occupations,

$$p_J=(e^{-\beta\mu_J}+1)^{-1}, \quad J=L,R, \tag{1}$$

where μ_L and μ_R are the respective reservoir chemical potentials, and $\beta=1/k_BT$. Rate equations for the averaged site occupations $p_l(t)$ $(l=1,\ldots,M)$ are given by

$$\frac{dp_l}{dt}=\langle j_{l-1,l}\rangle_t-\langle j_{l,l+1}\rangle_t, \tag{2}$$

where $\langle j_{l,l+1}\rangle_t$ for $l=0,\ldots,M$ denotes the net average current from site l to $l+1$, to be derived from the underlying master equation. Note that $\langle j_{0,1}\rangle_t\equiv\langle j_{L,1}\rangle_t$ and $\langle j_{M,M+1}\rangle_t\equiv\langle j_{M,R}\rangle_t$ are currents from the left and to the right reservoir. In order to proceed, we need to specify the rates for configurational transitions consistent with the detailed balance condition. We adopt here symmetric rates

$$w_{i,f}\propto\exp[\beta(E_i-E_f)/2], \tag{3}$$

where E_i and E_f is the total energy in the initial and final state, respectively. In particular, "bare" transition rates for elementary hops from l to $l\pm1$, which govern the single particle dynamics in the dilute limit, are given by $k_{l,l\pm1}(t)=\nu_{l,l\pm1}\exp[\beta(\varepsilon_l(t)-\varepsilon_{l\pm1}(t))/2]$. Here $\nu_{l,l\pm1}$ are frequency factors, which for simplicity are assumed independent of l for $l=1,\ldots,M-1$ and represent the bulk frequency ν_B, while at the system boundary we distinguish $\nu_L=\nu_{0,1}=\nu_{1,0}$ and $\nu_R=\nu_{M,M+1}=\nu_{M+1,M}$ from ν_B. Setting $(\nu_B)^{-1}=1$ and $\beta=1$ defines our units of time and energy.

Certain special cases of this model deserve special attention. For static site energies ε_l it describes aspects of passive transport, for example, through membrane channels.[21–23] Very recently, the nonlinear dc response and rectification in a single particle hopping system coupled to reservoirs were examined, including disorder effects.[24] Assuming $p_L\neq p_R$ but taking ε_l independent of both time and space, one recovers a generalized asymmetric simple exclusion process (ASEP) model[25] that contains a nearest neighbor coupling V (for reviews of the hard core repulsion ASEP as well as the totally asymmetric simple exclusion process model, see Refs. 26 and 27 and references therein).

Several driving modes, both stochastic and deterministic, that lead to unidirectional transport, were proposed in literature.[10,11] In this work we assume for simplicity a sinusoidal time dependence with frequency $\omega=2\pi/\tau$, which should allow us to study transport efficiencies as a function of the typical time scale set by the modulation period τ that characterizes the driving forces. With regard to the spatial asymmetry, common models are as follows:[11]

(a) peristaltic or traveling wavelike behavior, where potential minima move in one direction, thereby dragging particles with them;
(b) sawtoothlike potential with oscillating amplitude ("flashing ratchet"). In such systems particles are driven in the direction against the steeper potential slope.
(c) Constant (l-independent) ac-force ("rocking ratchet") superimposing a nonsymmetric static potential. Unidirectional transport directly results from steady state rectification properties of the static potential, as can be seen by considering the adiabatic limit $\omega\to0$.

The present work focuses on the first two mechanisms, (a) and (b). The model introduced above applies to multiply occupied channels driven by time-dependent mechanical forces, and working as motors or as chemical pumps. As specific examples we consider the following situations:

(i) *Motor action*: A constant load F is applied that changes the site energies relative to their intrinsic values $(\varepsilon_l)_{F=0}$,

$$\varepsilon_l=(\varepsilon_l)_{F=0}+\frac{Fl}{(M+1)}, \quad l=0,\ldots,M+1. \tag{4}$$

By this, the left and right reservoirs acquire a potential energy difference $\varepsilon_R-\varepsilon_L=F$, while their chemical potentials are taken equal, $p_R=p_L$.

(ii) *Chemical pump*: In a pure chemical pump the chemical potentials in the two reservoirs are different, e.g., $\mu_R>\mu_L(p_R>p_L)$, while the mechanical load F vanishes. Mathematically this case differs from model (4) by the fact that unlike the linear potential change in Eq. (4), the chemical potential difference $\mu_R-\mu_L$ will, in general, not give rise to a linear distribution of local chemical potential changes along the channel.

In both cases we can discuss different measures of machine performance and optimization schemes. First the output of the machine operation can be obtained from the average current

$$J_{\rm av}=\frac{1}{\tau}\int_0^\tau dt\frac{1}{M+1}\sum_{l=0}^{M}\langle j_{l,l+1}\rangle_t, \tag{5}$$

where, at steady state, the average (over realizations and over a modulation period τ) currents between neighboring positions do not depend on position. The useful work output is then

$$\bar{W}_{\rm out}=J_{\rm av}F \tag{6}$$

for the pure motor action, and

$$\bar{W}_{\text{out}} = J_{\text{av}}(\mu_R - \mu_L) \tag{7}$$

for the pure chemical pump. Note that combined effects of mechanical and chemical biases can be considered, in which case $\bar{W}_{\text{out}}=J_{\text{av}}(\mu_R^e-\mu_L^e)$ is the sum of Eqs. (6) and (7), the electrochemical potentials $\mu_{L,R}^e$ being defined according to Eq. (40). In all cases the work input can be calculated from

$$\bar{W}_{\text{in}} = \frac{1}{\tau}\int_0^\tau dt \sum_{l=1}^{M} \frac{d\varepsilon_l(t)}{dt} p_l(t). \tag{8}$$

This yields the conventional "efficiency"[28]

$$\eta = \frac{\bar{W}_{\text{out}}}{\bar{W}_{\text{in}}}. \tag{9}$$

Aiming for maximum efficiency is one criterion for optimization. Alternatively, irrespective of the amount of input energy, one can ask for the maximum F, where J_{av} changes sign ("reversal potential"), or for the maximum current $J_{\text{av}}>0$ against the load $F>0$, corresponding to the maximum rate of transfer of particles from L to R.

III. FOUR-SITE MODEL

Setting $M=2$, we have a four-site system consisting of a channel with sites $l=1,2$ in contact with boundary sites L and R. In this minimal ratchet model open to reservoirs the system is driven by modulating the site energies $\varepsilon_1(t)$ and $\varepsilon_2(t)$. An incipient peristaltic modulation of site energies can be realized by a phase lag in the oscillation of $\varepsilon_2(t)$ relative to $\varepsilon_1(t)$,

$$\varepsilon_L = 0, \tag{10}$$

$$\varepsilon_1(t) = \varepsilon_1^{(0)} + A[1+\sin(\omega t)] + F/3, \tag{11}$$

$$\varepsilon_2(t) = \varepsilon_2^{(0)} + A[1+\sin(\omega t - \pi/2)] + 2F/3, \tag{12}$$

$$\varepsilon_R = F. \tag{13}$$

Here, the energies $\varepsilon_l^{(0)}$ represent a constant energy shift of the channel's interior relative to the reservoirs. On the other hand, the in-phase oscillation where Eqs. (11) and (12) are replaced by

$$\varepsilon_1(t) = \varepsilon_1^{(0)} + 2A[1+\sin(\omega t)] + F/3, \tag{14}$$

$$\varepsilon_2(t) = \varepsilon_2^{(0)} + A[1+\sin(\omega t)] + 2F/3 \tag{15}$$

[keeping Eqs. (10) and (13)], corresponds to a "flashing" ratchet of the type of a discrete "sawtooth" potential. Both of these driving modes favor a current to the right.

Unidirectional flow induced by such driving schemes can be most simply investigated in the independent particle model where the average site occupations $p_1(t)$ and $p_2(t)$ evolve according to the linear rate equations

$$\frac{dp_1}{dt} = k_{L,1}(t)p_L - k_{1,L}(t)p_1 + k_{2,1}(t)p_2 - k_{1,2}(t)p_1, \tag{16}$$

$$\frac{dp_2}{dt} = k_{R,2}(t)p_R - k_{2,R}(t)p_2 - k_{2,1}(t)p_2 + k_{1,2}(t)p_1, \tag{17}$$

with prescribed populations $p_{L,R}$ at the boundary sites. A more realistic model should take into account interparticle interactions. Here we consider both hard core (site exclusion) and nearest neighbor interactions, denoted by V.

The following section (Sec. IV) describes an approximate approach to the kinetics of such models based on the (classical) time-dependent density functional theory. An exact approach, feasible for the present small system, is based on rate equations written in the system states representation. A system state (n_1,n_2) is defined in terms of the occupations of sites $l=1$ and $l=2$. Obviously our system is fully characterized by the four states—(0,0), (1,0), (0,1), and (1,1)—with the following corresponding energies:

$$E_{10}(t) = \varepsilon_1(t), \tag{18}$$

$$E_{01}(t) = \varepsilon_2(t), \tag{19}$$

$$E_{11}(t) = \varepsilon_1(t) + \varepsilon_2(t) + V. \tag{20}$$

E_{00} may conveniently be set to 0. We assume that transitions between these states proceed only by single particle steps so that no direct transition takes place between states (0,0) and (1,1). It should be emphasized that in using these energies to determine rates one needs to take into account the change of energy in the reservoir. Thus, the total energy change ΔE for the transition $(0,0)\to(1,0)$ is $E_{10}-\varepsilon_L=\varepsilon_1-\varepsilon_L$ and ΔE for the transition $(1,0)\to(1,1)$ is $E_{11}-E_{10}-\varepsilon_R=\varepsilon_2+V-\varepsilon_R$. The kinetic equations for the average population of these system states are

$$\frac{dP_{10}(t)}{dt} = K_{00,10}(t)P_{00}(t) + K_{01,10}(t)P_{01}(t) + K_{11,10}(t)P_{11}(t) - (K_{10,00}(t) + K_{10,01}(t) + K_{10,11}(t))P_{10}(t), \tag{21}$$

$$\frac{dP_{01}(t)}{dt} = K_{00,01}(t)P_{00}(t) + K_{10,01}(t)P_{10}(t) + K_{11,01}(t)P_{11}(t) - (K_{01,00}(t) + K_{01,10}(t) + K_{01,11}(t))P_{01}(t), \tag{22}$$

$$\frac{dP_{11}(t)}{dt} = K_{10,11}(t)P_{10}(t) + K_{01,11}(t)P_{01}(t) - (K_{11,10}(t) + K_{11,01}(t))P_{11}(t), \tag{23}$$

and normalization implies that

$$P_{00} = 1 - (P_{10} + P_{01} + P_{11}). \tag{24}$$

Using Eq. (24) in Eqs. (21)–(23) yields three inhomogeneous equations with rates that are readily obtained from Eq. (3) and Eqs. (18)–(20). Clearly, $K_{01,10}(t)=k_{2,1}(t)$ and $K_{10,01}(t)=k_{1,2}(t)$. The remaining rates involve the bath densities, for example,

$$K_{10,00}(t) = \nu_L \exp[\beta(\varepsilon_1(t) - \varepsilon_L)/2](1 - p_L), \tag{25}$$

$$K_{00,10}(t) = \nu_L \exp[-\beta(\varepsilon_1(t) - \varepsilon_L)/2]p_L. \tag{26}$$

Once the solutions to Eqs. (21)–(24) have been found, the average populations of individual sites are obtained from

$$p_1(t) = P_{10}(t) + P_{11}(t), \tag{27}$$

$$p_2(t) = P_{01}(t) + P_{11}(t), \tag{28}$$

and the currents $J_L(t) \equiv \langle j_{L,1}\rangle_t$; $J_R(t) \equiv \langle j_{2,R}\rangle_t$ can be calculated from, e.g.,

$$J_L(t) = K_{00,10}P_{00} - K_{10,00}P_{10} + K_{01,11}P_{01} - K_{11,01}P_{11}, \tag{29}$$

$$J_R(t) = K_{01,00}P_{01} - K_{00,01}P_{00} + K_{11,10}P_{11} - K_{10,11}P_{10}. \tag{30}$$

Note that results based on Eqs. (21)–(24) differ from those of the independent particle model, Eqs. (16) and (17), even in the limit $V=0$ because unlike the latter they incorporate hard core interactions. The behavior based on Eqs. (16) and (17) is expected only in the highly dilute limit when particle encounters on the same site are negligible.

IV. TDFT

TDFT is a local equilibrium approximation, in which the nonequilibrium character of the distribution function is manifested in the space- and time-dependent local fields acting on the single particle density. Given a distribution function of this type, density functional theory assumes that correlators determining the currents $\langle j_{l,l+1}\rangle_t$ in Eq. (2) are functionals of the single particle density; moreover, this functional dependence is the same as in the equilibrium case. This allows us to express the mean currents in Eq. (2) in terms of the densities $p_l(t)$ and therefore to arrive at a closed system of nonlinear rate equations. In the present problem this latter step can be carried through exactly because the free energy functional for one-dimensional lattice gases with short range interactions is known.[29,30]

Rate equation (2) for the averaged site occupations $p_l(t)$ $(l=1,2)$ in the four-site model reduces to

$$\frac{dp_1}{dt} = \langle j_{L,1}\rangle_t - \langle j_{1,2}\rangle_t, \tag{31}$$

$$\frac{dp_2}{dt} = \langle j_{1,2}\rangle_t - \langle j_{2,R}\rangle_t. \tag{32}$$

From the general formulation given in Appendix for channels with arbitrary length M in the presence of symmetric rate (3), we obtain by specializing to the present model with $M=2$,

$$\langle j_{L,1}\rangle_t = (1 - p_1 + Kp_{2,1}^{(3)})\left[\tilde{k}_{L,1}e^{\beta\mu_L} - \tilde{k}_{1,L}\left(\frac{p_{2,1}^{(2)}}{p_{2,1}^{(4)}}\right)\right], \tag{33}$$

$$\langle j_{1,2}\rangle_t = k_{1,2}p_{2,1}^{(2)} - k_{2,1}p_{2,1}^{(3)}, \tag{34}$$

$$\langle j_{2,R}\rangle_t = (1 - p_2 + Kp_{2,1}^{(2)})\left[\tilde{k}_{2,1}\left(\frac{p_{2,1}^{(3)}}{p_{2,1}^{(4)}}\right) - \tilde{k}_{R,2}e^{\beta\mu_R}\right], \tag{35}$$

with $K=\sqrt{\zeta}-1$; $\zeta=e^{-\beta V}$ (for details, see Appendix). For the sake of simplified notation, time arguments on the right hand side of these and subsequent equations are suppressed. The nearest neighbor correlators $p_{2,1}^{(n)}$ in these equations are defined by Eq. (A16) with $l=1$. Note that they are directly related to the average occupations of system states. Indeed, $P_{11}=p_{2,1}^{(1)}$, $P_{01}=p_{2,1}^{(2)}$, $P_{10}=p_{2,1}^{(3)}$, and $P_{00}=p_{2,1}^{(4)}$. Following the Appendix, the two- point correlator $p_{2,1}^{(1)} \equiv \langle n_2 n_1\rangle$ is explicitly found as

$$p_{2,1}^{(1)}(t) = \frac{1}{2(1-\zeta)}[(p_1+p_2)(1-\zeta) - 1 + \sqrt{[(p_1+p_2)(1-\zeta)-1]^2 + 4p_1p_2\zeta(1-\zeta)}]. \tag{36}$$

Clearly, setting all currents (33)–(35) equal to zero implies the equilibrium condition $\varepsilon_L+\mu_L=\varepsilon_R+\mu_R$ between both reservoirs. This is seen most directly from the underlying Eq. (A8).

In the limit $V\to 0$ one recovers $p_{2,1}^{(2)} \to p_1p_2$. Then Eqs. (33)–(35) become

$$\langle j_{L,1}\rangle_t = k_{L,1}(t)p_L(1-p_1(t)) - k_{1,L}(t)p_1(t)(1-p_L), \tag{37}$$

$$\langle j_{1,2}\rangle_t = k_{1,2}(t)p_1(t)(1-p_2(t)) - k_{2,1}(t)p_2(t)(1-p_1(t)), \tag{38}$$

$$\langle j_{2,R}\rangle_t = k_{2,R}(t)p_2(t)(1-p_R) - k_{R,2}(t)p_R(1-p_2(t)), \tag{39}$$

showing that site blocking effects are incorporated in a mean-field like manner. For general V, effective blocking factors for sites $l=1,2$ can be read directly from Eqs. (33) and (35). Considering site 1, the effective blocking factor that appears in the current $\langle j_{L,1}\rangle_t$ is $1-p_1+Kp_{2,1}^{(3)}$, which reduces to $1-p_1$ for $V=0$ and to $1-(p_1+p_2)$ for $V\to\infty$ because $p_{2,1}^{(1)}\to 0$ in the latter case. Hence, for $V\to\infty$ the occupation of the nearest neighbor site, p_2, enters into the effective blocking factor additively with p_1. The last conclusion follows from Eq. (36) provided that $p_1+p_2<1$, which obviously holds for $V\to\infty$ provided that μ_R and μ_L stay finite.[31] By this, and based on the identification $P_{11}\equiv p_{2,1}^{(1)}$, it is straightforward to show that for $V\to\infty$ the expressions for currents (33)–(35) and hence all results from TDFT become equivalent with those of Sec. III in the same limit (i.e., for $P_{11}\to 0$). A similar conclusion holds for $V\to-\infty$, where $K_{10,11}\to\infty$. According to Eq. (23) this limit requires that $P_{10}\to 0$. Similarly, $P_{01}\to 0$, and $P_{11}=p_1=p_2=1$ independent of time is seen to be a consistent solution. In this limit all currents are zero as the channel is jammed by the presence of two particles. On the other hand, Eq. (36) predicts that $p_{2,1}^{(1)} \to \max(p_1,p_2)$, which becomes unity since $p_1,p_2\to 1$. It follows that the TDFT correctly yields zero currents in this limit.

The following section provides a quantitative test of TDFT against the exact results obtained from Eqs. (21)–(24). When applied to the four-site model, this approximate

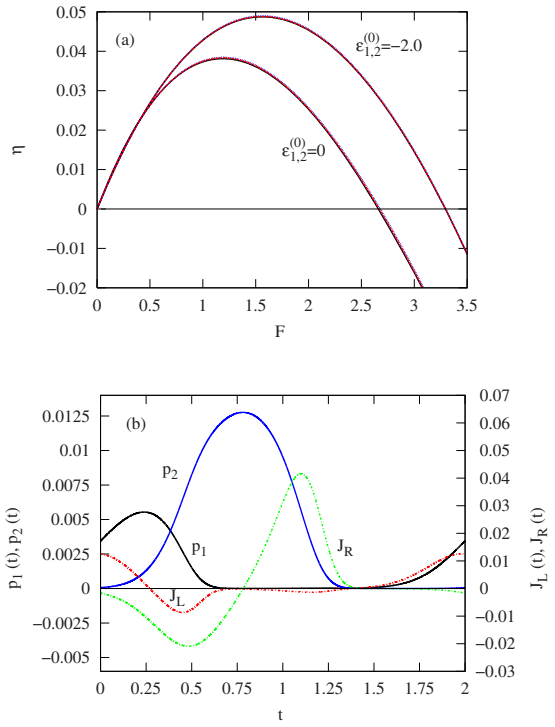

FIG. 1. Properties of a dilute system with $p_L=p_R=0.0067$ ($\mu_{L,R}=-5.0$), driving period $\tau=2$ and amplitude $A=5$. The behavior of this dilute system does not depend on V for $V=0$, 1, and 10, and results from the TDFT approximation are indistinguishable from the exact ones. Efficiency η as a function of mechanical bias $F=\varepsilon_R-\varepsilon_L$ ($\varepsilon_L=0$) (a). Lower curve: neutral static site energies, $\varepsilon^{(0)}_{1,2}=0$. Upper curve: attractive static site energies $\varepsilon^{(0)}_{1,2}=-2.0$. Time-dependent occupation probabilities $p_1(t)$, $p_2(t)$, and currents $J_{L,R}(t)$ for $\varepsilon^{(0)}_{1,2}=-2.0$ and $F=1.5$ (b). Shown is one period of stationary oscillation, where $t=0$ corresponds to a minimum in $\varepsilon_1(t)$, see Eq. (11).

method is not simpler than the exact treatment; however, its advantage lies in the immediate applicability to chains of arbitrary length M.[32]

V. RESULTS

A. Peristaltic driving, dilute limit

Now we investigate a 1D open channel under peristaltic driving by numerically solving Eqs. (21)–(24) in Sec. III and Eqs. (31)–(36) in Sec. IV with the input Eqs. (10)–(13). We first consider the dilute limit, approached by setting $\mu_L=\mu_R=-5$, i.e., $p_L=p_R\approx 0.0067$. Calculated efficiencies as a function of the mechanical load F show a maximum before they drop to zero and to negative values (current reversal), see Fig. 1. Clearly, for strong dilution, site blocking effects and the interaction V become irrelevant. Hence, the efficiency curves in Fig. 1 become indistinguishable from the predictions of the independent particle model equations (16) and (17). Also in this dilute limit, the TDFT results in Sec. IV perfectly agree with the numerical solutions of the exact equations (21)–(24). Indeed, in this limit P_{11} becomes negligibly small, and, as one can easily verify, both the exact equations (21)–(24) and the TDFT equations (31)–(35) become fully equivalent to the linear rate equations (16) and (17).

Figure 1(a) also reveals a significant enhancement of the efficiency for a channel which is made more attractive relative to the reservoirs, by changing the static part of site energies in Eq. (11) from $\varepsilon^{(0)}_{1,2}=0$ to $\varepsilon^{(0)}_{1,2}=-2.0$. The value $\varepsilon^{(0)}_{1,2}=-2.0$ is therefore used in all our subsequent calculations with peristaltic driving. Apparently, attracting more particles to the channel interior overcompensates for the effect of a less favorable exit rate $k_{2,R}$.

Direct insight into the peristaltic mechanism is gained from Fig. 1(b). During a time window where $\varepsilon_1(t)\lesssim 1$ particles from the left reservoir have access to the channel so that the left current $J_L(t)$ and $p_1(t)$ increase with time. [This happens for $1.5\lesssim t\lesssim 2$ in the plot of Fig. 1(b).] During the subsequent upward movement of level 1 density from this level flows both back to the reservoir, rendering $J_L(t)<0$, and in the forward direction to level 2, which is lower in energy because of the phase lag $\pi/2$ between both levels. Therefore $p_2(t)$ increases, but as long as $\varepsilon_2(t)\lesssim 1$ there is also a flow to level 2 from the right reservoir, reflected by the negative peak in the right current $J_R(t)$. This influx from the right is the reason why the p_2-peak actually gets higher than the p_1-peak. Upward movement of level 2 in turn causes the subsequent positive peak in $J_R(t)$, while a decay of $p_2(t)$ to the left is prohibited as long as $\varepsilon_2(t)<\varepsilon_1(t)$. The peaks in the time-dependent densities and currents can be shown to be more pronounced for $\varepsilon^{(0)}_{1,2}=-2$ in comparison with $\varepsilon^{(0)}_{1,2}=0$, leading to the increased efficiency displayed in Fig. 1(a) for the more attractive channel. Since during the upward movement of level 1 its population decays both toward the left and right, we expect that this mechanism can translocate a particle with probability not larger than about 0.5 within one cycle.

B. Peristaltic driving, moderately dense system, $p_L=p_R$

Figure 1(b) shows that at low densities, a large amplitude peristaltic oscillation, Eqs. (10)–(13), tends to locate particles on that site which momentarily has lower energy. This is evident from the figure as the overlap of the two peaks for $p_1(t)$ and $p_2(t)$ is small. Figures 2 and 3 show results obtained at higher densities, imposed by setting $p_L=p_R=0.5(\mu_L=\mu_R=0)$, where effects of correlations between transporting particles are expected. At these densities the overlap between the $p_1(t)$ and $p_2(t)$ peaks is larger, as seen in the case $V=0$ in Figs. 3(a) and 3(b), which show slightly broader peaks and overlap regions than in Fig. 1(b). Consequently, many-body effects become important, as discussed below.

It may be intuitively expected that simultaneous presence of particles on both sites 1 and 2 should cause reduction of pump efficiency because these particles block each other, impairing the peristaltic driving. Hence one expects that efficiency will increase as V changes from attractive ($V<0$) to repulsive ($V>0$), where double occupation of the channel is increasingly suppressed. These arguments are supported by calculations of η and J_{av} for nondilute systems. Figure 2 shows results for $p_{L,R}=0.5$, obtained from both the exact method described in Sec. III, and the TDFT approximation,

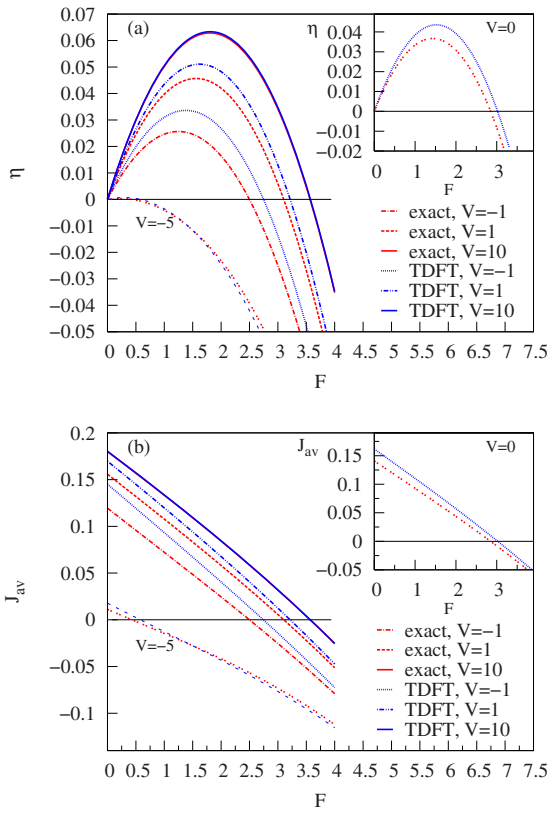

FIG. 2. F-dependent efficiency η (a) and averaged current J_{av} (b) for different interparticle interactions V in a driven channel coupled to moderately dense reservoirs with $p_L=p_R=0.5$ ($\mu_{L,R}=0$). Other parameters are $\varepsilon_{1,2}^{(0)}=-2.0$, $\tau=2$, and $A=5.0$. The insets show the $V=0$ case, where interparticle interactions arise from site exclusion only, and the main figure shows results for $V=-5$, -1, 1, and 10. Shown are results from the exact kinetic equations (red lines) and from the TDFT (blue lines).

Sec. IV. Before addressing the quality of the TDFT approximation, let us focus on the main features in Fig. 2 common to both treatments.

Comparing the $V=0$ case[33] shown in the inset in Fig. 2(a) with the independent particle results [dilute limit, Fig. 1(a)] we indeed observe that mere site blocking leads to a decrease in η. This trend in η is enhanced for increasingly negative V (attractive interparticle interactions) but is reversed with increasingly positive (repulsive) V, again in agreement with the above expectation. Interestingly, for $V=10$, η significantly exceeds the result for the dilute limit discussed before, see Fig. 1(a), by about 30%. One should note that a strong repulsion as in the case $V=10$ is practically equivalent to the condition that the two-site channel can only be singly occupied or vacant. This "single particle limit" appears to optimize active transport in our model.

Similar conclusions hold with respect to the average current J_{av}, plotted against F in Fig. 2(b). The current increases for increasingly repulsive (positive) V and becomes negligibly small for increasingly attractive interaction. For $V=10$ the reversal potential (the load F for which J_{av} vanishes) is larger by about 15% than the corresponding value in the case $V=0$. For strong attractive interaction, e.g., $V=-5$, see Fig. 2, both current and efficiency are strongly damped.

Regarding the comparison of both methods, it is evident from Fig. 2 that the TDFT can well account for important qualitative features in our model of a driven open channel. At $V=0$, the TDFT becomes identical to ordinary mean-field theory because all correlators factorize, leading to Eqs. (37)–(39). One should note that quite generally nontrivial and even long range correlations can be induced in systems when driven far away from equilibrium.[34,35] Such correla-

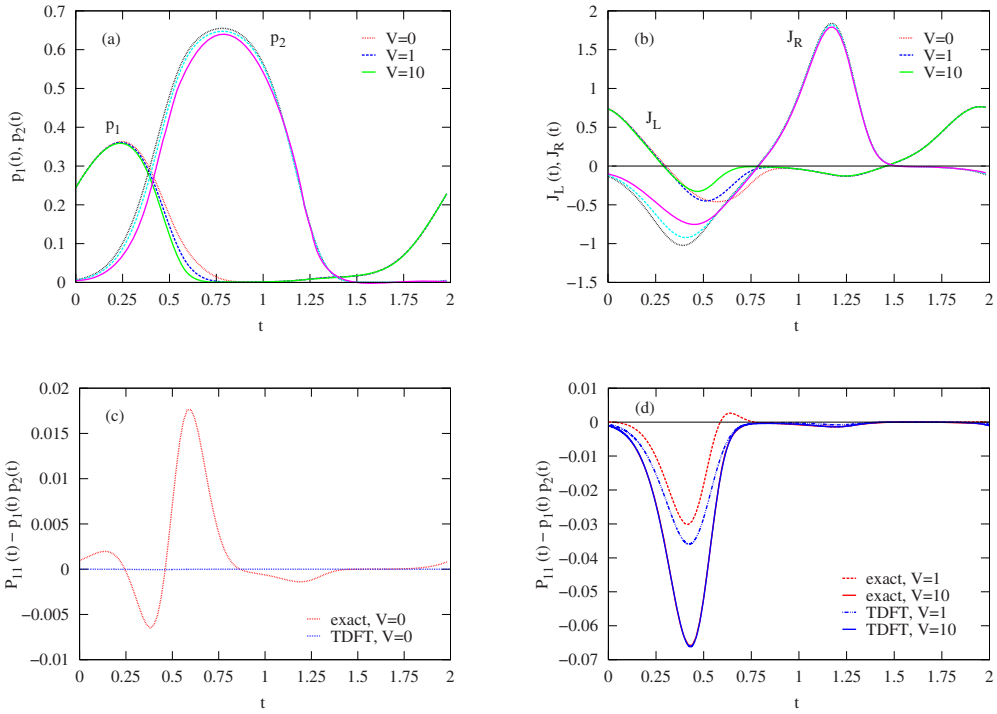

FIG. 3. Exact time-dependent occupation probabilities $p_{1,2}(t)$ (a), left and right currents (b), as well as correlation function $P_{11}(t)-p_1(t)p_2(t)$ for different $V\geq 0$ [(c) and (d)] in a nondilute system with $p_{L,R}=0.5$ and $F=1.5$. Other parameters are as in Fig. 2. Plots (c) and (d) illustrate the differences between exact correlations and local equilibrium correlations assumed in the TDFT.

tions are ignored in the TDFT approach. From the inset in Fig. 2, we see that for $V=0$ TDFT overestimates the maximum efficiency η by about 14% relative to the exact calculation. This error shrinks when V increases from zero because the TDFT accounts for the concomitant suppression of double occupation of the channel. For strong coupling, $V \gg 1$, the TDFT applied to our model asymptotically becomes exact because as discussed before in Sec. IV, it correctly describes the one-particle limit.

For practical applications, attractive interactions are less interesting than repulsive ones since they tend to immobilize a pair of particles on sites 1 and 2, thus diminishing the current. For the sake of comparison of the two methods, however, we have included in Fig. 2 examples with $V<0$. An almost quantitative accuracy of the TDFT is observed when the attraction becomes as strong as $V=-5$, again in accord with the previous analytical arguments in Sec. IV.

The development of correlations inside the channel of the type discussed above is illustrated in Figs. 3(c) and 3(d), which show the difference $P_{11}(t)-p_1(t)p_2(t)$ within one driving period. The load is taken as $F=1.5$, where the corresponding efficiencies are close to their maximum. For $V=0$, see Fig. 3(a), peaks of either sign appear in the exact results in parallel with the peaks in $p_1(t)$ and $p_2(t)$, but they are narrower than the latter. On average, these current-induced nonequilibrium correlations are positive, i.e., attractive. However, already under the mild repulsive interaction, $V=1$, the negative peak takes over. For strong repulsion, P_{11} practically vanishes so that the curve for $V=10$ simply reflects the negative product of the densities p_1 and p_2. Obviously, the TDFT reproduces such correlations better for larger V.

The influence of the driving period τ (in fact $\tau\nu_B$ as discussed above) is displayed in Fig. 4. Unless otherwise specified, here and in the following we only show the exact results from Sec. III. In all cases studied, however, we have verified that the TDFT performs with similar accuracy as for the foregoing plots. Obviously, except for the driving mode itself, the driving period is a fundamental parameter that determines the pump performance. For our model both the efficiency η and the current J_{av} go through a maximum as a function of τ. To maximize η, a smaller load requires slower driving, as seen in Fig. 4(a). Increasing F, the maxima in η shift to shorter τ. On the other hand, from the point of view of maximizing J_{av}, even shorter τ are required, e.g., $\tau \simeq 1.2$ for $F=2$ [see Fig. 4(b)]. This illustrates that optimization of pump performance, in general, depends on the optimization criterion for a particular application. The choice $\tau=2$ in most of our calculations is found to be a good compromise between these different optimization criteria. Yet another criterion might be to maximize the number of particles transmitted within one cycle, which is τJ_{av}. Figure 4(b) suggests that in our model this number will be limited by about 0.5, as argued before. It should also be noted that τ-dependent efficiencies and the peak structure in the J_{av} versus τ curves qualitatively agree with Refs. 15 and 16, where a model based on repulsive on-site interactions and periodic boundary conditions was considered.

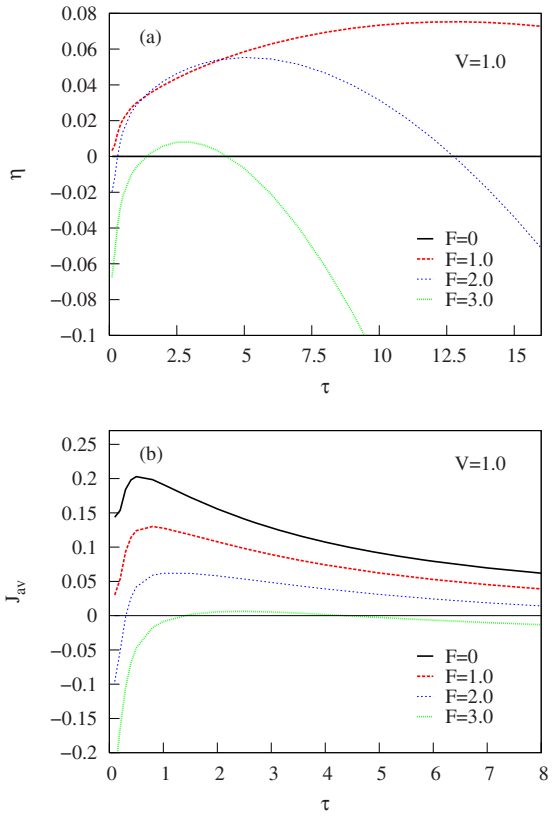

FIG. 4. Efficiency η (a) and averaged current J_{av} (b) from exact rate equations as a function of τ for $p_{L,R}=0.5$, $V=1$, and different $F=0$, 1, 2, and 3. Other parameters as in Fig. 2.

C. Peristaltic pump: Effect of chemical driving, $p_L \neq p_R$

It is well-known that passive transport in the linear response regime at constant temperature is governed solely by the gradient in the external electrochemical potential

$$\mu^e = F + \mu. \tag{40}$$

Far from equilibrium, however, the mechanical and chemical potentials F and μ play separate roles in determining the kinetics. This difference stems from the different ways at which these imposed biases are expressed inside the channel. The "mechanical bias" $F=\varepsilon_R-\varepsilon_L$ is assumed to fall linearly along the channel, as described by Eqs. (10)–(15), while the chemical bias $\Delta\mu=\mu_R-\mu_L$ is assumed to affect only the external reservoirs R and L. Therefore, the average current J_{av} in our model depends differently on these two external variables, $J_{\mathrm{av}}=J_{\mathrm{av}}(F,\Delta\mu)$. This is illustrated in Fig. 5, where the current is plotted versus the difference $\Delta\mu^e=\mu_R^e-\mu_L^e$ in the electrochemical potentials of the two reservoirs under different partitionings of $\Delta\mu^e$ with respect to the mechanical and chemical load. In these calculations $p_L=0.1$ is fixed ($\mu_L \approx -2.197$), whereas $p_R \geq p_L$ is variable upon varying $\Delta\mu$. Shown are only the two limiting cases $J_{\mathrm{av}}(0,\Delta\mu)$ and $J_{\mathrm{av}}(F,0)$, labeled as $F=0$ and $\Delta\mu=0$, respectively. Note that in biophysical systems pumping of charged ions across a membrane will generate a voltage drop so that, in principle, the full two-variable characteristics $J_{\mathrm{av}}(F,\Delta\mu)$ will enter. As seen from Fig. 5(a), the current $J_{\mathrm{av}}(0,\Delta\mu)$ for small bias is less sensitive to changes in $\Delta\mu$ in comparison with the

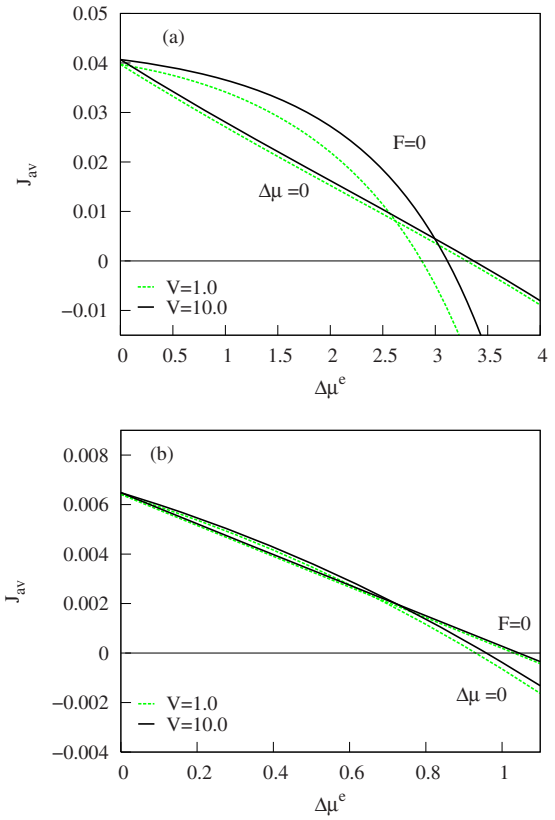

FIG. 5. The average current J_{av} from the exact rate equations in a peristaltic pump as a function of the electrochemical potential difference $\Delta\mu^e=F+\Delta\mu$ between the two reservoirs, for $V=1$ and 10 (a). Other parameters are as in Fig. 2: $\varepsilon_{1,2}^{(0)}=-2.0$, $\tau=2$, and $A=5.0$. Compared are the two limiting cases $J_{\mathrm{av}}(F,0)$, where $\Delta\mu=0$ and $J_{\mathrm{av}}(0,\Delta\mu)$, where $F=0$. In either case the left density is fixed to $p_L=0.1$ ($\mu_L\approx-2.197$). Same for a flashing ratchet with $\varepsilon_{1,2}^{(0)}=-1.0$, $\tau=2$, and $A=2.0$ (b).

F-dependence of $J_{\mathrm{av}}(F,0)$. This is because after time averaging, p_R enters the net current from site 2 to R mainly through the blocking factor $1-p_R$ in Eq. (25), implying only a mild p_R-dependence. However, when $p_R\gtrsim0.5$ the current $J_{\mathrm{av}}(0,\Delta\mu)$ drops more steeply toward negative values than $J_{\mathrm{av}}(F,0)$. In contrast, as in Fig. 3, the drop in $J_{\mathrm{av}}(F,0)$ down to the reversal potential is not far from linear. The corresponding TDFT results were found to be in excellent agreement with these results. Note that the small concentration $p_L=0.1$ implies that the interaction V has only a minor influence on $J_{\mathrm{av}}(F,0)$.

The difference in the channel's response under a chemical versus mechanical load also becomes apparent when we compare the respective efficiencies, which are plotted in Fig. 6 against $\Delta\mu^e=\mu_R^e-\mu_L^e$. As for Fig. 5 we have taken $p_L=0.1$ fixed and p_R variable. The chemical efficiency, defined by Eqs. (9) and (7), is displayed by the curves labeled $F=0$. Their maxima and the corresponding chemical reversal potentials are systematically lower than those referring to the mechanical efficiency ($\Delta\mu=0$, $F\neq0$).

D. Flashing ratchet potential

An important question is to what extent the previous results for peristaltic driving will change when the drive mode changes. We exemplify this for the flashing ratchet

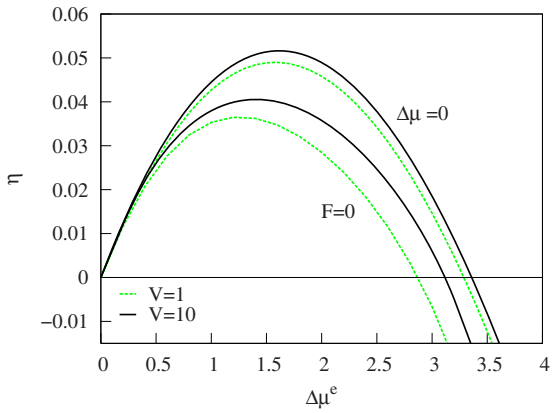

FIG. 6. Chemical efficiency ($F=0$) compared with mechanical efficiency ($\Delta\mu=0$) for peristaltic driving, both as a function of $\Delta\mu^e=F+\Delta\mu$ and for different V. The left density is fixed to $p_L=0.1$ ($\mu_L\approx-2.197$). Other parameters as in Fig. 5(a).

potential, Eq. (14). Here we use the parameters $A=2.0$ and $\varepsilon_{1,2}^{(0)}=-1.0$ that correspond to a maximum in $\varepsilon_2(t)$ of the same height relative to the bath levels as for peristaltic driving with $A=5.0$ and $\varepsilon_{1,2}^{(0)}=-2.0$. Figure 7 shows F-dependent mechanical efficiencies η and currents J_{av}. The qualitative appearance of the curves including their dependence on V is analogous to Fig. 2, but the absolute performance is considerably worse than for peristaltic driving. The efficiency η and the average current J_{av} are seen to be lower by about an order of magnitude and a factor of 5, respectively, in the flashing driving mode. Thereby we have verified that choos-

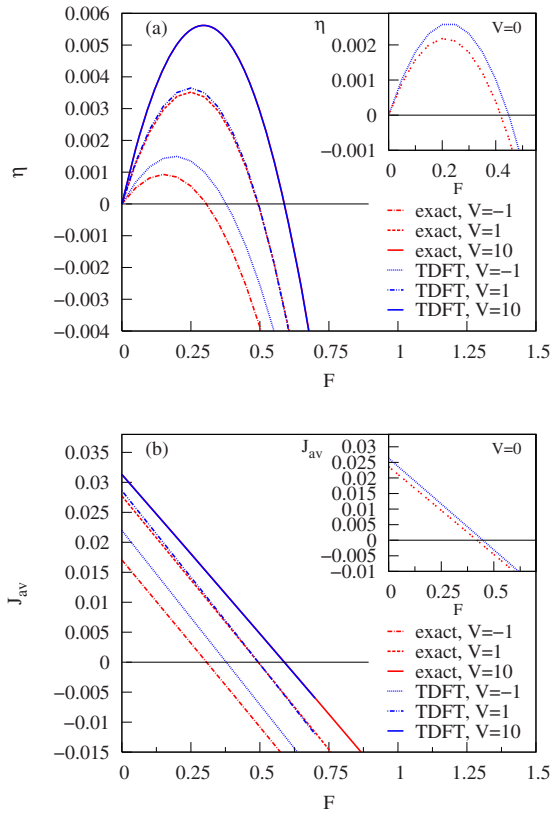

FIG. 7. Efficiency (a) and average current (b), plotted against the bias F for a flashing ratchet in the moderately dense system characterized by $p_L=p_R=0.5$ ($\mu_{L,R}=0$). Other parameter are $\varepsilon_{1,2}^{(0)}=-1.0$, $\tau=2$, and $A=2.0$.

ing $\tau=2$, the efficiency curves $\eta(F)$ in Fig. 7 are near optimum. We also computed the analog to Fig. 5(a) for the flashing ratchet, see Fig. 5(b). Currents again are much smaller than in Fig. 5(a). A notable feature is the near agreement of the curves for chemical ($F=0$) and mechanical ($\Delta\mu=0$) bias, presumably because of a fairly regular distribution of induced local chemical potential changes along the channel in the case of the sawtooth potential.

VI. SUMMARY AND CONCLUSIONS

Active transport was studied within a stochastic model for an open two-site channel, driven by time-dependent site energies and coupled to left and right reservoirs. Exact rate equations for this problem were established and solved numerically. Despite the simplicity of our model, it allowed us to examine important conditions for efficient transport, which we expect to be of relevance regarding both the design of synthetic active channel devices and, potentially, the functioning of biological motors and ion pumps.

The main findings which emerge from our investigations are summarized as follows.

(i) Because of the coupling to reservoirs with prescribed chemical potentials, the number of particles inside the channel fluctuates, allowing multiple channel occupation. As a consequence, transport depends on interparticle interactions, described by a local hard core repulsion and a nearest neighbor interaction constant V. V-dependent motor and pump efficiencies are studied systematically, showing that they become optimized when multiple occupation of the channel gets suppressed by a large repulsive V. As intuitively expected, this effect saturates and the efficiencies become independent of interparticle interaction when $V\to\infty$. In particular, the $V=10$ results displayed in Fig. 2 were found to represent this saturation limit. On the other hand, choosing an even higher modulation amplitude ($A=10$ instead of $A=5$ used in the foregoing calculations for peristaltic driving), the maximum efficiency was found to increase only slightly, whereas the reversal potential increases considerably. These results, including a decrease of η under attractive interactions $V<0$, were derived for a short channel ($M=2$). By contrast, as shown in Ref. 13, for attracting particles high efficiencies can arise in long channels in the presence of a long-wavelength ratchet-type potential, an effect connected with condensation of particles around the potential minima.

(ii) Different performance criteria can be formulated, based, for example, on an economical use of the input energy in producing mechanical or chemical work (efficiencies η), or on maximizing the output "power," i.e., the current. These measures of efficiency, as defined in this paper, are not intrinsic properties of the system, but obviously depend on the imposed load. It is also possible to define an intrinsic measure, η_s, of an "ideal" efficiency by (for a mechanical bias; a similar definition can be used in the chemical bias case)

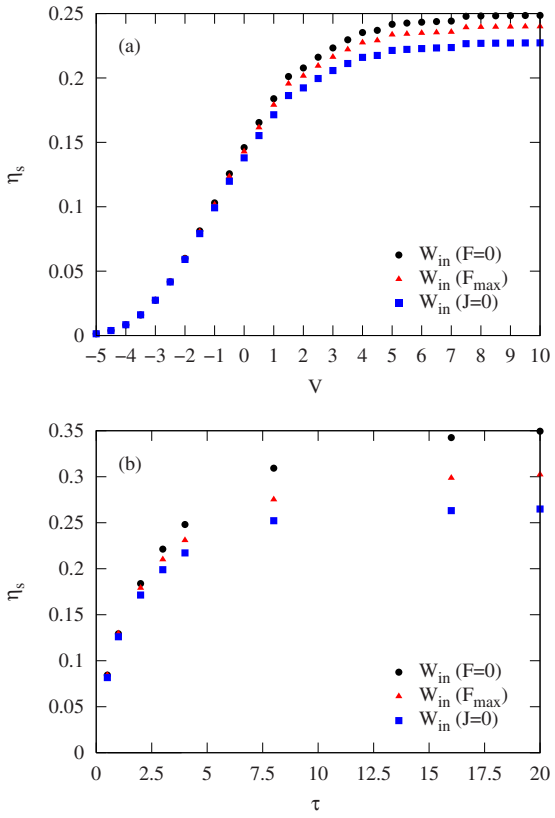

FIG. 8. The ideal efficiency η_s displayed as a function of the interparticle coupling V using $\tau=2$ (a) and of the modulation time τ using $V=1$ (b), for a peristaltic pump with $\varepsilon_{1,2}^{(0)}=-2.0$, $A=5$, and three different choices for calculating $\bar{W}_{in}$: at $F=0$, $J=0$, and at $F=F_{max}$, where the efficiency η defined by Eq. (9) is maximal.

$$\eta_s=\frac{J_{av}(F=0)F(J=0)}{\bar{W}_{in}(F=0)}, \tag{41}$$

where $J_{av}(F=0)$ is the flux at zero bias while $F(J=0)$ is the mechanical bias for which the current vanishes. The product $J_{av}(F=0)F(J=0)$ is the analog of the product of the short-circuit current and the open-circuit voltage that provides an upper bound to the useful work that can be extracted from a given voltage source. The choice of $\bar{W}_{in}(F=0)$ as the denominator in Eq. (41) is to some extent arbitrary since the input work in our model is defined through the energy absorbed by the system (in contrast to situations encountered, e.g., in photovoltaic devices, where the input work is defined by the incident rather than the absorbed energy). Other choices, e.g., using $\bar{W}_{in}(J=0)$ as denominator in Eq. (41) could be made. As shown in Fig. 8 these different definitions yield different results for what may be regarded as the ideal machine performance. In either case, the performance is sensitive to the interparticle coupling and to the driving period τ, and different efficiency criteria require different τ for optimization.

(iii) In the far from equilibrium processes considered here, generated currents depend on the partitioning of the electrochemical potential difference $\Delta\mu^{(e)}=F+\Delta\mu$ between the reservoirs in terms of the mechanical and

chemical loads F and $\Delta\mu$. In other words, these biasing attributes play different roles in the kinetics.

(iv) Peristaltic driving reflected by a phase shift in the oscillating site energies yields much better performances than an oscillating sawtoothlike potential (flashing ratchet).

Some of these findings, in particular, the possibility of efficiency enhancement by repulsive interactions and the above-mentioned dependencies on the driving period, agree on a qualitative level with earlier work,[15,16] despite considerable differences in the model design and in details of the results. We take this as an indication that the corresponding conclusions formulated above should hold rather generally.

It would certainly be interesting to extend these investigations to longer channels, with the aim to analyze collective effects in overdamped systems under time-dependent driving. The full problem based on the master equation, however, soon becomes intractable as the length M increases. Results based on the TDFT nicely agree with the exact solutions for $M=2$, suggesting that this approximation could yield reliable results also for arbitrary channel lengths. The underlying equations of motion for arbitrary M are presented in the Appendix and will be evaluated in forthcoming work.

It should be emphasized that unlike equilibrium properties, the behavior of the system in nonequilibrium steady states depends, sometimes sensitively, on the assumed kinetic model. We have repeated some of the calculations for two more kinetic models, a normalized kinetic model, where the rates between two levels with energy separation $\Delta E>0$ are taken to be

$$k\begin{pmatrix}\text{up}\\ \text{down}\end{pmatrix}=\frac{e^{\mp(\beta/2)\Delta E}}{e^{(\beta/2)\Delta E}+e^{-(\beta/2)\Delta E}} \tag{42}$$

and an asymmetric model where

$$k(\text{up})=\frac{e^{-(\beta/2)\Delta E}}{1+e^{-(\beta/2)\Delta E}},\quad k(\text{down})=\frac{1}{1+e^{-(\beta/2)\Delta E}}. \tag{43}$$

Because rates based on Eq. (42) or Eq. (43) are smaller than those from Eq. (3), longer modulation periods are needed in order to get similar behavior. Apart from this rescaling of τ the qualitative behavior of these models remains as with our original model, Eq. (3).

Some other important questions are deferred to future work. In addition to the average currents studied in the present paper, current fluctuations are observed in experimental studies of channel transport, and their theoretical evaluation is of interest. In particular, generalizing available methodologies for carrier counting statistics to models with time-dependent driving provides an interesting direction for future investigation. A more ambitious task would be to generalize the concept advanced in the paper to the quantum regime. Indeed, ratchet action inducing driving in quantum transport has been discussed, so far for systems of noninteracting carriers.[11,36] Consideration of quantum effects in more general setups—see, e.g., Ref. 37—may be proven useful in the discussion of novel energy transfer systems.

ACKNOWLEDGMENTS

M.E. gratefully acknowledges funding by a Forschungsstipendium by the Deutsche Forschungsgemeinschaft (DFG) (Grant No. EI 859/1-1). M.E. and W.D. have greatly benefited from numerous discussions with Philipp Maass. W.D. is also grateful to the Max-Planck-Institut fuer Physik Komplexer Systeme, Dresden, for its hospitality. A.N. acknowledges support by the European Science Council (FP7/ERC) (Grant No. 226628), the Israel-Niedersachsen Research Fund, and the Israel Science Foundation. He also thanks the Alexander von Humboldt Foundation for sponsoring his visit at the University of Konstanz. A.N. and G.S. thank Mark Ratner for many helpful discussions. This work was also supported by the Non-equilibrium Energy Research Center (NERC) which is an Energy Frontier Research Center funded by the U.S. Department of Energy, Office of Science, Office of Basic Energy Sciences under Award No. DE-SC0000989. The authors also wish to thank the Lion Foundation for supporting this work.

APPENDIX: CURRENTS FROM THE TDFT APPROACH

In this appendix we recall the main steps of the TDFT for Fermionic lattice gases.[17–19] At the same time we generalize the derivation to systems with arbitrary time-dependent site energies ε_i and kinetic properties governed by a class of transition rates, where

$$w_{i\to k}(\mathbf{n})=\nu_{i,k}n_i v_k g(H_i,H_k) \tag{A1}$$

represents the rate for a particle hop from site i to a nearest neighbor site k. Occupation numbers are denoted by n_l with $n_l=0$ or 1, $v_l=1-n_l$ and $\mathbf{n}\equiv\{n_l\}$. $\nu_{i,k}$ are frequency factors. The function g depends on the energies H_i and H_k of the particle before and after the hop, respectively. Focusing on this transition between sites i and k, the total lattice gas Hamiltonian is decomposed as

$$H(\mathbf{n})=H_{i,k}+n_iH_i+n_kH_k+n_in_kV_{i,k}, \tag{A2}$$

where $V_{i,k}$'s are pair interaction parameters. $H_{i,k}$ denotes the total energy omitting contributions from sites i and k, while

$$H_i=\varepsilon_i-\mu_{\text{tot}}+\sum_{l\neq(i,k)}V_{i,l}n_l. \tag{A3}$$

Here μ_{tot} is some reference chemical potential.

Clearly, $H_{i,k}$, H_i, and H_k depend only on occupational configurations $\hat{\mathbf{n}}$ excluding sites i and k. For the following it is convenient to introduce the quantity

$$G_{i,k}(\hat{\mathbf{n}})=g(H_i,H_k)\exp(-\beta H_i), \tag{A4}$$

which, by the detailed balance condition, is required to be symmetric in its indices,

$$G_{i,k}(\hat{\mathbf{n}})=G_{k,i}(\hat{\mathbf{n}}). \tag{A5}$$

If transition rates depend only on the particle's initial energy,[18] then $G_{ik}(\hat{\mathbf{n}})\equiv 1$. On the other hand, calculations in this work are based on the symmetric choice $g(H_i,H_k)=\exp[\beta(H_i-H_k)/2]$ or

$$G_{i,k}(\hat{\mathbf{n}}) = \exp[-\beta(H_i + H_k)/2]. \tag{A6}$$

The TDFT is based on a local equilibrium approximation for the distribution function,

$$P^{\mathrm{loc}}(\mathbf{n},t) = \frac{1}{Z(t)}\exp[-\beta H^{\mathrm{eff}}(\mathbf{n},t)];$$
$$H^{\mathrm{eff}}(\mathbf{n},t) = H(\mathbf{n}) + \sum_l h_l(t)n_l. \tag{A7}$$

Its nonequilibrium character is represented in terms of time-dependent single particle fields $h_l(t)$ that are associated with the time-dependent local chemical potential, see Eq. (A11). In view of Eqs. (A1)–(A5) and using $n_i^2 = n_i$ ($n_i v_i = 0$), the average current from i to k can be expressed as

$$\begin{aligned}\langle j_{i,k}\rangle_t &= \nu_{i,k}\sum_{\mathbf{n}}[n_i v_k g(H_i,H_k) - v_i n_k g(H_k,H_i)]P^{\mathrm{loc}}(\mathbf{n},t)\\ &= \nu_{i,k}\sum_{\mathbf{n}} G_{i,k}(\hat{\mathbf{n}})[n_i v_k - v_i n_k]\exp[-\beta(h_i n_i + h_k n_k)]\\ &\quad\times\exp(-\beta H_{i,k}^{\mathrm{eff}}(\hat{\mathbf{n}})),\end{aligned}$$

where $H_{i,k}^{\mathrm{eff}}$ is the first term in (A2) when applied to the corresponding decomposition of H^{eff}. Summation over n_i and n_k yields

$$\langle j_{i,k}\rangle_t = M_{i,k}(t)[A_i(t) - A_k(t)] \tag{A8}$$

where

$$A_i(t) = \exp[-\beta(h_i(t) - \mu_{\mathrm{tot}})] \tag{A9}$$

and

$$M_{i,k}(t) = \frac{\nu_{i,k}}{Z(t)}\sum_{\hat{\mathbf{n}}} G_{i,k}(\hat{\mathbf{n}})e^{-\beta H_{i,k}^{\mathrm{eff}}(\hat{\mathbf{n}})}e^{-\beta\mu_{\mathrm{tot}}}.$$

The summation over $\hat{\mathbf{n}}$ can be continued to a summation over all $\mathbf{n}$ after including vacancy occupation numbers for sites i and k. Thus

$$M_{i,k}(t) = \nu_{i,k}\langle v_i v_k G_{i,k}(\hat{\mathbf{n}})\rangle_t e^{-\beta\mu_{\mathrm{tot}}}, \tag{A10}$$

which is symmetric, $M_{i,k}(t) = M_{k,i}(t)$, in view of Eq. (A4). Note that μ_{tot} cancels in Eq. (A10). Density functional theory is employed when computing average densities $p_i(t) \equiv \langle n_i\rangle_t$ from Eq. (A7). The result is the "structure equation"

$$\varepsilon_i + h_i + \mu_i(\mathbf{p}) = \mu_{\mathrm{tot}}, \tag{A11}$$

which allows us to eliminate h_i in favor of the local chemical potential $\mu_i(\mathbf{p}) = \partial F/\partial p_i$; $F(\mathbf{p})$ being the free energy functional associated with $H(\mathbf{n})$, with $\mathbf{p} = \{p_l\}$ (for details, see Ref. 18). It follows that

$$A_i(t) = \exp[\beta(\varepsilon_i + \mu_i)], \tag{A12}$$

which can be interpreted as local activity. The essence of Eq. (A8) now becomes obvious, namely, a factorization of the average current into a thermodynamic factor (difference of local activities) and the kinetic coefficient (A10). A closed system of equations determining $p_i(t)$ is obtained by combining Eqs. (A8)–(A12) with the equation of continuity

$$\frac{dp_i(t)}{dt} + \sum_k \langle j_{i,k}\rangle_t = 0. \tag{A13}$$

Now we apply that method to the model of Sec. II, which is a finite one-dimensional channel of M sites with nearest neighbor interactions, coupled to reservoirs L and R. From Eqs. (A6) and (A10) we obtain

$$\begin{aligned}M_{l,l+1}(t) &= \nu_{l,l+1}\exp[-\beta(\varepsilon_l + \varepsilon_{l+1})/2]\\ &\quad\times\langle v_l v_{l+1}\exp[-\beta(V_{l-1,l}n_{l-1} + V_{l+1,l+2}n_{l+2})/2]\rangle_t,\end{aligned} \tag{A14}$$

where $V_{l-1,l} = V$ for $l = 2,\ldots,M$. Note that the reservoirs were taken to have no interaction with the channel, $V_{0,1} \equiv V_{L,1} = 0$ and $V_{M,M+1} \equiv V_{M,R} = 0$. Moreover, it exactly holds that[18]

$$\beta\mu_l(\mathbf{p}) = \ln\frac{p_l}{1-p_l} + \ln\frac{(1-p_l)p_{l+1,l}^{(2)}}{p_l p_{l+1,l}^{(4)}} + \ln\frac{(1-p_l)p_{l,l-1}^{(3)}}{p_l p_{l,l-1}^{(4)}}. \tag{A15}$$

The correlators $p_{l+1,l}^{(n)}$ are defined by

$$p_{l+1,l}^{(2)} \equiv \langle v_{l+1}n_l\rangle = p_l - p_{l+1,l}^{(1)}, \tag{A16}$$

$$p_{l+1,l}^{(3)} \equiv \langle n_{l+1}v_l\rangle = p_{l+1} - p_{l+1,l}^{(1)}, \tag{A17}$$

$$p_{l+1,l}^{(4)} \equiv \langle v_{l+1}v_l\rangle = 1 - p_l - p_{l+1} + p_{l+1,l}^{(1)}, \tag{A18}$$

where $v_l = 1 - n_l$ is the vacancy occupation number. These quantities $p_{l+1,l}^{(n)}$ can be determined[18] from the "quasichemical condition" $p_{l+1,l}^{(1)}p_{l+1,l}^{(4)} = p_{l+1,l}^{(2)}p_{l+1,l}^{(3)}e^{-\beta V}$ by solving a quadratic for, e.g., $p_{l+1,l}^{(1)} = \langle n_{l+1}n_l\rangle$. Equation (A15) is written as a sum of three terms such that the first term corresponds to a noninteracting lattice gas, while the second (third) term is the contribution of the right (left) neighbor to the chemical potential at site i.

Equations (A14) and (A15) together with Eq. (A12) determine the currents (A8) in the interior of the system. Evidently, Eq. (A14) involves higher order correlators, actually up to four-point correlators because of $\exp(\alpha n) = 1 + n(\exp\alpha - 1)$ for $n = 0$ or 1. Knowing $F(\mathbf{p})$, these correlators can be expressed[38] as functionals of $\mathbf{p}$.

The average currents from and to the reservoirs require special attention. First, because interactions between the system and reservoirs are disregarded, the chemical potentials for the outermost sites $l = 1$ and $l = M$ of the channel satisfy

$$\beta\mu_1(\mathbf{p}) = \ln\frac{p_{2,1}^{(2)}}{p_{2,1}^{(4)}}, \quad \beta\mu_M(\mathbf{p}) = \ln\frac{p_{M,M-1}^{(3)}}{p_{M,M-1}^{(4)}}. \tag{A19}$$

This follows from the fact that all correlators in Eq. (A15) involving reservoir sites factorize so that in Eq. (A15) contributions of the interactions between sites $l = 1, M$ and the reservoirs vanish. Second, the kinetic coefficients that enter the currents between the system and the reservoirs are obtained from [using Eq. (A14)]

$$M_{L,1}(t) = \nu_L \exp\left[-\beta\left(\frac{\varepsilon_L + \varepsilon_1}{2}\right)\right]\langle v_L\rangle\left\langle v_1 \exp\left(-\beta\frac{Vn_2}{2}\right)\right\rangle_t. \tag{A20}$$

Using again $\exp(\alpha n)=1+n(\exp\alpha-1)$, the last factor in Eq. (A20) simplifies

$$\left\langle v_1 \exp\left(-\beta\frac{Vn_2}{2}\right)\right\rangle = 1 - p_1 + Kp_{2,1}^{(3)}, \tag{A21}$$

with $K=\exp(-\beta V/2)-1$. An expression analogous to Eq. (A20) is obtained for $M_{M,R}(t)$.

After insertion of Eqs. (A19)–(A21) into Eqs. (A12) and (A8) we obtain

$$\langle j_{L,1}\rangle_t = (1 - p_1 + Kp_{2,1}^{(3)})\left[\tilde{k}_{L,1}e^{\beta\mu_L} - \tilde{k}_{1,L}\left(\frac{p_{2,1}^{(2)}}{p_{2,1}^{(4)}}\right)\right], \tag{A22}$$

where $\langle v_L\rangle$ has been absorbed in the attempt frequency entering $\tilde{k}_{L,1}$ and $\tilde{k}_{1,L}$ by setting $\tilde{\nu}_L=\langle v_L\rangle\nu_L$.

Similarly,

$$\langle j_{M,R}\rangle_t = (1 - p_M + Kp_{M,M-1}^{(2)}) \times\left[\tilde{k}_{M,R}\left(\frac{p_{M,M-1}^{(3)}}{p_{M,M-1}^{(4)}}\right) - \tilde{k}_{R,M}\exp(\beta\mu_R)\right], \tag{A23}$$

with $\tilde{\nu}_R=\langle v_R\rangle\nu_R$ in the definition of $\tilde{k}_{R,M}$ and $\tilde{k}_{M,R}$. Note that apart from modified attempt frequencies $\tilde{\nu}_{L,R}$, the only reservoir properties entering the theory are the chemical potentials $\mu_{L,R}$. In this way and by using Eq. (A13), we end up with a closed system of equations for an open channel of arbitrary length, coupled to reservoirs.

Specializing to the four-site model ($M=2$) of Sec. III, the above expressions for the reservoir currents coincide with Eqs. (33) and (35) in the main text. Moreover, to get the current $\langle j_{1,2}\rangle_t$ inside the two-site channel, we use Eq. (A14) to obtain

$$M_{1,2}(t) = \nu \exp\left[-\beta\left(\frac{(\varepsilon_1 + \varepsilon_2)}{2}\right)\right]\langle v_1 v_2\rangle_t, \tag{A24}$$

with $\langle v_1 v_2\rangle_t \equiv p_{2,1}^{(4)}$. Together with Eq. (A19), this leads to Eq. (34).

[1] F. Jülicher, A. Ajdari, and J. Prost, Rev. Mod. Phys. **69**, 1269 (1997).
[2] P. Läuger, *Electrogenic Ion Pumps* (Sinauer Associates, Sunderland, MA, 1991).
[3] B. Hille, *Ionic Channels of Excitable Membranes*, 3rd ed. (Sinauer Associates, Sunderland, MA, 2001).
[4] E. Muneyuki and T. A. Fukami, Biophys. J. **78**, 1166 (2000).
[5] V. Kaila, M. Verkhovsky, G. Hummer, and M. Wikström, Proc. Natl. Acad. Sci. U.S.A. **105**, 6255 (2008).
[6] J. Rousselet, L. Salome, A. Ajdari, and J. Prost, Nature (London) **370**, 446 (1994).
[7] Z. Siwy and A. Fuliński, Phys. Rev. Lett. **89**, 198103 (2002).
[8] M. Galperin, M. A. Ratner, and A. Nitzan, Nano Lett. **5**, 125 (2005).
[9] B. L. Altshuler and L. I. Glazman, Science **283**, 1864 (1999).
[10] P. Reimann, Phys. Rep. **361**, 57 (2002).
[11] P. Hänggi and F. Marchsoni, Rev. Mod. Phys. **81**, 387 (2009).
[12] I. Derényi and T. Vicsek, Phys. Rev. Lett. **75**, 374 (1995).
[13] S. Savel'ev, F. Marchesoni, and F. Nori, Phys. Rev. E **71**, 011107 (2005).
[14] P. Reimann, R. Kawai, C. Van den Broeck, and P. Haenggi, Europhys. Lett. **45**, 545 (1999).
[15] F. Slanina, Europhys. Lett. **84**, 50009 (2008).
[16] F. Slanina, J. Stat. Phys. **135**, 935 (2009).
[17] D. Reinel and W. Dieterich, J. Chem. Phys. **104**, 5234 (1996).
[18] M. Kessler, W. Dieterich, H. L. Frisch, J. F. Gouyet, and P. Maass, Phys. Rev. E **65**, 066112 (2002).
[19] J. F. Gouyet, M. Plapp, W. Dieterich, and P. Maass, Adv. Phys. **52**, 523 (2003).
[20] In the continuum limit, and under the assumption of symmetric hopping rates this method has been shown (Ref. 19) to become equivalent with dynamic density functional theory (Refs. 39 and 40) used in soft matter physics, see also Ref. 41.
[21] A. B. Kolomeisky, Phys. Rev. Lett. **98**, 048105 (2007).
[22] A. M. Berezhkovskii and S. M. Bezrukov, Phys. Rev. Lett. **100**, 038104 (2008).
[23] A. Zilman, J. Pearson, and G. Bel, Phys. Rev. Lett. **103**, 128103 (2009).
[24] M. Einax, M. Körner, P. Maass, and A. Nitzan, Phys. Chem. Chem. Phys. **12**, 645 (2010).
[25] M. Dierl, P. Maass, and M. Einax (in preparation).
[26] B. Derrida, Phys. Rep. **301**, 65 (1998).
[27] G. Schütz, in *Phase Transitions in Critical Phenomena*, edited by C. Domb and J. Lebowitz (Academic, San Diego, 2001), Vol. 19, pp. 1–251.
[28] K. Sumithra and T. Sintes, Physica A **297**, 1 (2001).
[29] J. K. Percus, Acc. Chem. Res. **27**, 224 (1994).
[30] J. Buschle, P. Maass, and W. Dieterich, J. Phys. A **33**, L41 (2000).
[31] If $p_1+p_2>1$, a situation that can be reached if μ_L and/or μ_R approach infinity at finite interaction V, a different solution is obtained as $V\to\infty$ that is not considered here.
[32] M. Einax (in preparation).
[33] Since the numerator and denominator in Eq. (36) become zero for $\zeta=0$, the TDFT results labeled $V=0$ are actually for $V=0.001$.
[34] H. Spohn, J. Phys. A **16**, 4275 (1983).
[35] B. Derrida, J. Stat. Mech.: Theory Exp. 2007, P07023.
[36] J. Lehmann, S. Kohler, P. Hänggi, and A. Nitzan, Phys. Rev. Lett. **88**, 228305 (2002).
[37] J. Cao and R. J. Silbey, J. Phys. Chem. A **113**, 13825 (2009).
[38] R. Evans, Adv. Phys. **28**, 143 (1979).
[39] U. Marini Bettolo Marconi and P. Tarazona, J. Chem. Phys. **110**, 8032 (1999).
[40] P. Español and H. Löwen, J. Chem. Phys. **131**, 244101 (2009).
[41] W. Dieterich, H. L. Frisch, and A. Majhofer, Z. Phys. B: Condens. Matter **78**, 317 (1990).